IJMMM International Journal of Minerals, Metallurgy and Materials 矿物冶金与材料学报（英文版）

Solid Bi_2O_3-derived nanostructured metallic bismuth with high formate selectivity for the electrocatalytic reduction of CO_2

Xiaoyan Wang, Safeer Jan, Zhiyong Wang, and Xianbo Jin

Cite this article as:
Xiaoyan Wang, Safeer Jan, Zhiyong Wang, and Xianbo Jin, Solid Bi_2O_3-derived nanostructured metallic bismuth with high formate selectivity for the electrocatalytic reduction of CO_2, *Int. J. Miner. Metall. Mater.*, 31(2024), No. 4, pp. 803-811. https://doi.org/10.1007/s12613-023-2770-y

View the article online at SpringerLink or IJMMM Webpage.

INTERNATIONAL JOURNAL OF
Minerals, Metallurgy and Materials

Volume 31, Number 4, April 2024
Page 803

Research Article https://doi.org/10.1007/s12613-023-2770-y

Solid Bi_2O_3-derived nanostructured metallic bismuth with high formate selectivity for the electrocatalytic reduction of CO_2

Xiaoyan Wang[1)], *Safeer Jan*[1)], *Zhiyong Wang*[1)], *and Xianbo Jin*[1,2),✉]

1) College of Chemistry and Molecular Sciences, Hubei Key Laboratory of Electrochemical Power Sources, Wuhan University, Wuhan 430072, China
2) Engineering Research Center of Organosilicon Compounds & Materials, Ministry of Education, Wuhan 430072, China
(Received: 22 July 2023; revised: 26 October 2023; accepted: 31 October 2023)

Abstract: CO_2 electrochemical reduction (CO_2ER) is an important research area for carbon neutralization. However, available catalysts for CO_2 reduction are still characterized by limited stability and activity. Recently, metallic bismuth (Bi) has emerged as a promising catalyst for CO_2ER. Herein, we report the solid cathode electroreduction of commercial micronized Bi_2O_3 as a straightforward approach for the preparation of nanostructured Bi. At −1.1 V versus reversible hydrogen electrode in a $KHCO_3$ aqueous electrolyte, the resulting nanostructure Bi delivers a formate current density of ~40 mA·cm^{-2} with a current efficiency of ~86%, and the formate selectivity reaches 97.6% at −0.78 V. Using nanosized Bi_2O_3 as the precursor can further reduce the primary particle sizes of the resulting Bi, leading to a significantly increased formate selectivity at relatively low overpotentials. The high catalytic activity of nanostructured Bi is attributable to the ultrafine and interconnected Bi nanoparticles in the nanoporous structure, which exposes abundant active sites for CO_2 electrocatalytic reduction.

Keywords: bismuth; carbon dioxide; electrocatalysis; formate; solid electroreduction

1. Introduction

The electroreduction of CO_2 to fuels is desirable for constructing a carbon-cyclable energy system, particularly because renewable electricity is used for the electrolysis process [1]. However, CO_2, typically inert at room temperatures, requires a large overpotential to form the activated-state CO_2^{*-}, and the following reduction process suffers from slow kinetics [2]. Complicated proton-coupled multicharge transfer reactions and the competitive reduction of protons to hydrogen in an aqueous solution over most electrocatalysts will lead to various cathodic products [3]. Thus, developing electrocatalysts with high selectivity and high activity remains crucial.

Among various CO_2 electrochemical reduction (CO_2ER) products, formic acid (HCOOH) is particularly appealing, as it can serve as a fuel for combustion or in fuel cells, a hydrogen storage carrier, and a valuable raw chemical for industrial synthesis [4]. Regarding commercial viability, a techno-economic analysis revealed that HCOOH or formate was the most profitable product of CO_2ER [2]. A recent study reported that many metallic catalysts with high hydrogen evolution overpotential, including Cd, Pb, Hg, and Bi, showed high activity for CO_2ER [5]. Among these metallic catalysts, Bi stands out in terms of formate selectivity, and it is characterized by a relatively high elemental abundance and environmental friendliness [6–8]. Although Bi catalysts have shown high Faradaic efficiency (FE) for formate generation, the geometric productive rate of the Bi electrodes is still lower than the metrics required for practical application. Therefore, improving Bi catalyst activity without sacrificing selectivity is crucial.

Compared with bulk materials, nanostructured materials typically exhibit superior electrocatalytic performance because they facilitate the construction of highly porous electrodes with numerous active sites for CO_2 molecule adsorption [9–11]. Additionally, nanostructure metals with an integrity conductive network can improve the utilization rate of catalytic materials [12]. For example, porous Bi nanosheets have demonstrated high activity and formate selectivity in CO_2ER [6,13]. Beyond creating a nanoporous structure of the catalyst, researchers have tried to reduce the size of primary particles in the porous electrodes to increase the specific surface area of catalysts. A study on porous Ag demonstrated that as primary particle size decreased from 400 to 50 nm, the FE of CO increased from 75% to 82% under similar conditions [14]. Jia *et al.* [15] explored the influence of bismuth nanoparticle size on formic acid production, and the optimal catalyst yielded a formate FE higher than 90% within a potential window close to 400 mV. However, preparing nanostructure catalysts while maintaining the integrity of their conductive network is a rather complicated procedure.

Herein, nanostructured Bi (nBi) was prepared through facile electrochemical reduction of solid bismuth oxide (Bi_2O_3).

✉ Corresponding author: Xianbo Jin E-mail: xbjin@whu.edu.cn

Through the adjustment of the Bi_2O_3 particle size, nano Bi catalysts with different surface morphology and particle sizes were obtained. When used as an electrode catalyst for CO_2ER, Bi_2O_3-derived nBi yielded a formate FE approaching 98% at −0.78 V vs. reversible hydrogen electrode (RHE) and high stability over a 10 h electrolysis period. The straightforward preparation method and excellent electrocatalytic performance of nBi make the Bi_2O_3-derived nBi a desirable catalyst candidate for CO_2ER.

2. Experimental

2.1. Preparation of nBi catalysts

The nBi catalysts were synthesized through electrochemical reduction of a bismuth oxide electrode. To prepare the oxide electrode, bismuth oxide was rolled into a membrane (~0.1 mm in thickness, 5.1 mg·cm^{-2}) using 10wt% polytetrafluoroethylene (PTFE) as binder and isopropanol as solvent. Then, a rectangular piece (5 mm × 7 mm) of the membrane was pressed onto a titanium (Ti) mesh as a working electrode (WE) for constant-current reduction (5 mA) for 30 min in a 1.0 M K_2CO_3 solution against a graphite counter electrode (CE). The Ti mesh was used as the substrate, as it would not cause apparent currents for CO_2ER and hydrogen evolution [16]. Two types of nBi from bismuth oxide of different sources were prepared. One was derived from the as-received commercial bismuth oxide (purchased from Shanghai Reagent No. 2 Factory, China), with particles in the micrometer scale (denoted as mBO), and the prepared nBi was denoted as mBO-nBi. The other was derived from the self-made nanometer bismuth oxide (nBO) and was denoted as nBO-nBi. The nBO was synthesized via precipitation between bismuth nitrate pentahydrate and potassium hydroxide in aqueous solution. Specifically, 270 mg of $Bi(NO_3)_3\cdot 5H_2O$ was added to 1.0 mol·L^{-1} HNO_3, and then KOH was added under constant magnetic stirring. The resulting white precipitate was collected after water washing at least six times, and then, the nBO was dried in a vacuum oven at 60°C for further use. All chemicals were purchased from Sinopharm Chemical Reagent Company (China) unless otherwise specified.

2.2. Electrochemical reduction of CO_2

The electrochemical measurements were controlled by a CS350H electrochemical workstation (Wuhan, China) using a customized gas-tight H-cell. The anode and cathode chambers were separated by a Nafion 117 membrane (DuPont, the United States of America). The reference electrode was an Ag/AgCl (saturated KCl solution) electrode, and the CE was a Pt foil. A 0.5 M $KHCO_3$ electrolyte was utilized, and before CO_2ER tests, CO_2 gas was bubbled into the electrolyte for saturation. Potentials were calibrated to a RHE as E vs. RHE) = E vs. Ag/AgCl + 0.197 + 0.059 × pH.

Any gaseous products from the CO_2ER were collected and analyzed via gas chromatography (GC, Shandong Lunan Ruihong Chemical Instruments Co., Ltd., China). Liquid products were investigated via nuclear magnetic resonance (NMR, Bruker AVANCE III HD 400MHz, Germany) with calibration curves. Each quantitative analysis was performed three times under ambient pressure at 25°C, and an average result was reported.

The FEs for H_2, CO, and formate generation were calculated via the following equations:

$$FE_{CO(or\ H_2)} = \frac{a\times\left(\frac{v}{60}\right)\times N\times F\times\left(\frac{p}{RT}\right)}{i}\times 100\% \quad (1)$$

$$FE_{formate} = \frac{Q_{formate}}{Q_{total}}\times 100\% = \frac{N\times F\times n_{formate}}{i\times t} \quad (2)$$

where v (15 mL·min^{-1}) represents the flow rate of CO_2; a represents the concentration of CO (or H_2) determined via GC; $n_{formate}$ (mol) represents the molar amount of formate; N represents the electron transfer number for the generation of 1 mol formate, CO, or H_2; i (A) represents the reduction current during the CO_2ER process; t (s) represents the reduction time; $Q_{formate}$ and Q_{total} (C) represent the formate charge or total charge during the electrolysis, respectively; F represents the Faraday constant 96485 C·mol^{-1}; p = 1.013 × 10^5 Pa; T = 298.15 K; R = 8.314 J·K^{-1}·mol^{-1}.

2.3. Material characterizations

X-ray diffraction (XRD, Cu K_α radiation) analysis was conducted using the Bruker D8-advanced instrument (Bruker Corporation, Billerica, United States) or Rigaku Miniflex600 (Rigaku Corporation, Tokyo, Japan). The sample morphologies were imaged via scanning electron microscopy (SEM, SIRION 200 with a field-emission gun, the United States of America) and transmission electron microscopy (TEM, JEOL, and JEM-2100, Japan).

3. Results and discussion

3.1. Solid cathode reduction of mBO and nBO to nBi

Fig. 1 illustrates the nBi electrode preparation procedure. The as-received commercial micrometer Bi_2O_3 (mBO) or the homemade nanosize Bi_2O_3 (nBO) was used as the precursor. It was made into a membrane electrode and electrochemically reduced to form the nBi membrane electrode. Fig. S1(a) depicts the morphologies of the mBO and shows the aggregation of many Bi_2O_3 micrometer curved sheets. The commercial mBO sample was composed of Bi_2O_3 (PDF#, 71-2274) and trace impurities (Bi_2O_4 or $Bi_2O_2CO_3$), according to the XRD analysis (Fig. 2(a)). The impurities were probably caused by long-time exposure to the chemical in the atmosphere. The XRD pattern of the mBO membrane electrode subjected to electrochemical reduction in 1 M K_2CO_3 (Fig. 2(a)) shows only peaks of Bi (PDF#, 85-1329) and Ti; the peaks of Ti likely originated from the current collector. This indicates the complete conversion of mBO into Bi metal.

The surface of the as-rolled mBO membrane appeared dense (Fig. S1(c)). After electroreduction, the resulting mBO-nBi electrode exhibited a nanoporous structure com-

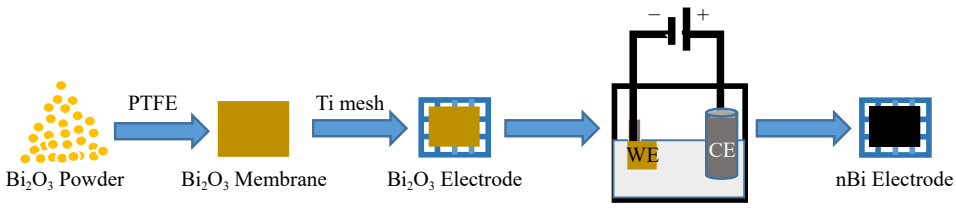

Fig. 1. Schematic of the nBi catalyst preparation process.

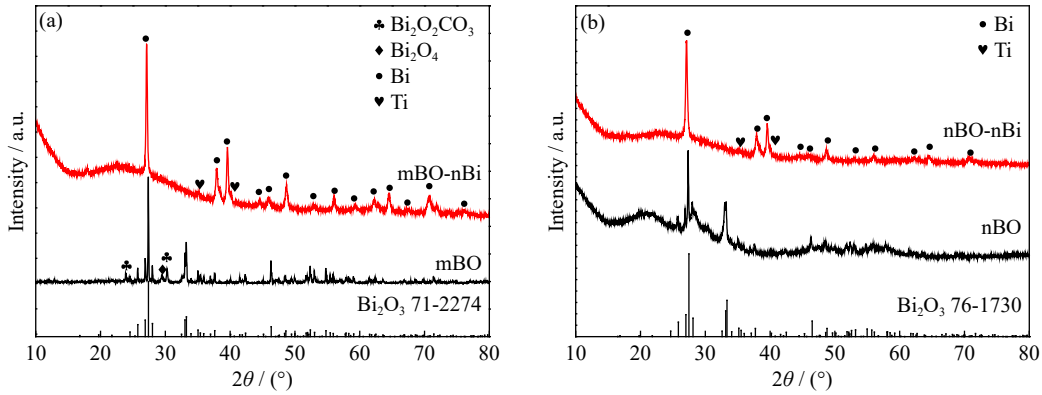

Fig. 2. XRD patterns: (a) mBO and the obtained mBO-nBi electrode; (b) the homemade nanometer Bi_2O_3 (nBO) and the obtained nBO-nBi electrode.

prising nBi dendrites with a primary particle size of ~80 nm (Fig. 3(a) and (b)). These nBi dendrites were tightly interconnected to form a nanostructure conductive network, likely advantageous for facilitating the mass transfer of CO_2 in the electrolytes during CO_2ER [12,17–19].

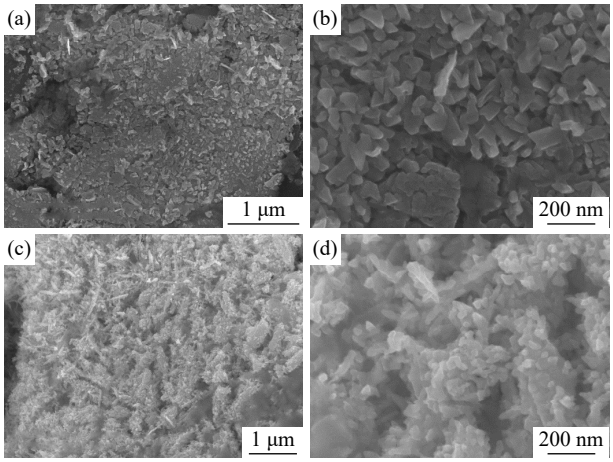

Fig. 3. Typical SEM images of the (a, b) mBO-nBi electrode and (c, d) nBO-nBi electrode.

To explore the influence of Bi_2O_3 particle sizes, homemade Bi_2O_3 consisting of nanoparticles was used as a mBO substitute, and the prepared nBi electrode was denoted as the nBO-nBi electrode. Fig. 2(b) displays the XRD pattern of the homemade Bi_2O_3. All of the diffraction peaks can be indexed to Bi_2O_3 (PDF#, 76-1730). In contrast, the synthesized Bi_2O_3 (Fig. S1(b)) was composed of nanorods with a diameter of ~30 nm, confirming the successful synthesis of nano bismuth oxide (nBO). Fig. 2(b) further confirms that after the electrochemical reduction, nBO was entirely converted to metallic bismuth (PDF#, 85-1329). SEM reveals the morphology change from the nBO membrane to the nBO-nBi electrode. The nBO membrane was dense (Fig. S1(d)). In the nBO-nBi electrode, needle-shaped dendritic Bi was hierarchically aligned on the Ti mesh surface to form a highly porous Bi network (Fig. 3(c)). Compared with the mBO-nBi electrode, the nBO-nBi electrode featured a smaller Bi particle size (approximately 30–50 nm, Fig. 3(d)). The TEM image of nBO-nBi (Fig. 4(a)) confirmed that nBO-nBi was composed of nanoparticles 30–50 nm in diameter. The lattice fringe spacing of the high-resolution TEM (HRTEM) image in Fig. 4(b) was 0.33 nm, corresponding to the Bi (012) plane, which proves that the solid electrochemical reduction of nBO led to the generation of metallic Bi nanoparticles.

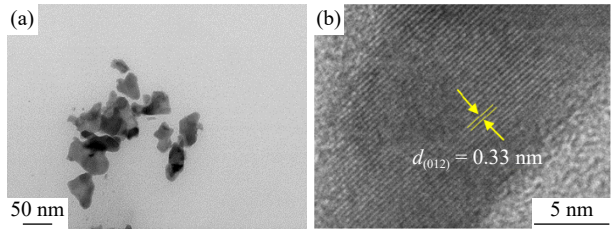

Fig. 4. (a) TEM image and (b) HRTEM image of nBO-nBi.

3.2. Electrocatalytic reduction of CO_2 with nBi catalysts

The electrochemical performances of the Bi_2O_3-derived nBi catalysts were investigated in the CO_2-saturated $KHCO_3$ electrolyte. Linear sweep voltammetry at 50 $mV \cdot s^{-1}$ was used to evaluate the influence of the catalysts on the reduction current. At potentials more negative than −0.7 V, the electrolyte in its natural state (i.e., without the addition of CO_2 gas) began to decompose at mBiO-nBi and nBiO-nBi electrodes (Fig. 5(a)). However, upon the bubbling of the CO_2 into the electrolyte, both catalysts yielded significantly larger cathodic current under the same potential as that of the case without

CO_2 addition. This suggests that nBi has a higher catalytic activity for CO_2ER than for the hydrogen evolution reaction (HER). In the CO_2-saturated $KHCO_3$ electrolyte, the reduction at the mBO-nBi electrode started at −0.65 V. In contrast, the onset potential at the nBO-nBi electrode was −0.62 V. Simultaneously, at −0.9 V, the cathodic reduction currents were −36 and −30 mA·cm^{-2} at the nBO-nBi and mBO-nBi electrode, respectively. The earlier onset potential and the larger cathodic current at the nBO-nBi electrode compared with those at the mBO-nBi electrode reveals the higher electrocatalytic activity of the nBO-nBi catalyst. Notably, the obtained reduction current of approximately −70 mA·cm^{-2} at the nBO-nBi electrode is nearly the highest reported current for CO_2ER based on an H-type cell [20–21].

However, high activity does not necessarily mean high catalyst selectivity, especially considering that the CO_2ER is complicated and has various products. The product selectivity of the two Bi catalysts was analyzed via constant-potential electrolysis of the CO_2-saturated $KHCO_3$ solution, and the products of CO_2ER based on the mBO-nBi and nBO-nBi electrodes were analyzed. The gas and liquid products were detected through GC and NMR, respectively. Three products, H_2, CO, and formate were detected. After the quantitative determination of the electrolyzed products generated at different potentials, the potential-dependent FEs of the three products, $FE_{formate}$, FE_{CO}, and $FE_{hydrogen}$, were calculated (Fig. 5(b) and (c)). The $FE_{formate}$ of the nBO-nBi electrode reached 81.7% at −0.63 V (Fig. 5(b)), higher than that of the mBO-nBi electrode (68%) under similar conditions. This study suggests that constructing an interlinked catalyst layer and reducing Bi particle size can improve the electrocatalytic activity of Bi for CO_2 reduction at a lower overpotential. The maximum FE achieved for formate generation was 97.2% (−0.74 V) and 97.6% (−0.78 V) for nBO-nBi and mBO-nBi, respectively, demonstrating the high formate selectivity of the nBi catalyst toward CO_2ER, consistent with the previous observation that the $FE_{formate}$ over the metallic Bi catalyst exceeded 90% [22–23]. Both nBi catalysts in the present study effectively suppressed CO generation, as indicated by an FE_{CO} of <7% (Fig. 5(c)) in the considered potential range. The nBO-nBi catalyst yielded $FE_{formate}$ higher than 80% at potentials of −0.63 to −0.98 V. The mBO-nBi catalyst yielded 80% $FE_{formate}$ at potentials of −0.65 to −1.1 V. When the potential shifted negatively to −1.18 V, the formate selectivity at the nBO-nBi electrode decreased to 52%. In comparison, the FE_{H_2} increased to 46%. However, the $FE_{formate}$ at the mBO-nBi electrode remained at 74% at −1.18 V.

The partial current of formate generation ($j_{formate}$, Fig. 5(d)) at the two nBi electrodes was calculated as the product of the $FE_{formate}$ (Fig. 5(b)) and the total reduction current (Figs. S2–S3). The nBO-nBi electrode yielded greater $j_{formate}$ than mBO-nBi at potentials more positive than −0.9 V. However, the nBO-nBi and mBO-nBi electrodes displayed similar $j_{formate}$ values under potentials more negative than −0.98 V, and the mBO-nBi electrode even outperformed the nBO-nBi electrode at −1.18 V in terms of $j_{formate}$ (~40 mA·cm^{-2}), owing to the sharp decrease in $FE_{formate}$ at the nBO-nBi electrode.

To analyze the reason for the difference in current densities delivered at different nBi electrodes during the CO_2ER, the electrochemical surface areas (ECSAs) of the two nBi

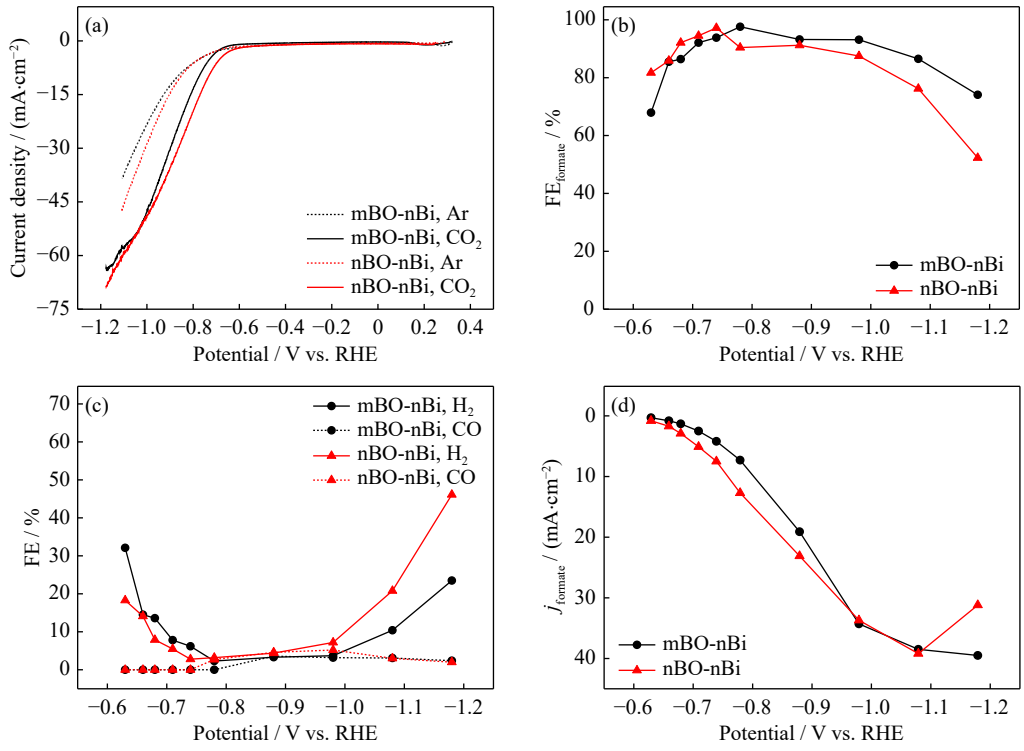

Fig. 5. (a) Linear scan (50 mV·s^{-1}) curves of the mBO–nBi and nBO–nBi electrodes in 0.5 M $KHCO_3$ before and after the bubbling of CO_2 gas. FEs of different products from CO_2 reduction: (b) formate; (c) CO and H_2. (d) Partial current density for formate production ($j_{formate}$) at different nBi electrodes.

electrodes were calculated according to double-layer charging capacities (Fig. 6). The double-layer charging capacity was measured via cyclic voltammetry at the double-layer potential domain (between −0.01 and −0.13 V). The double-layer charging currents for both electrodes were proportional to the scan rate, and the half-gap currents between the anodic and cathodic branches at −0.07 V were plotted against the scan rate (Fig. 6), forming perfect lines (Fig. 6(b) and (d)). The double-layer capacitance of the electrodes can be calculated via linear curve fitting, and it is linearly correlated with the ECSA of the electrode [24]. The double-layer capacitances of the nBO-nBi and mBO-nBi electrodes were approximately 4.45 and 1.98 mF·cm^{-2}, respectively, indicating that the nBO-nBi electrode had an ECSA more than twice that of the mBO-nBi electrode. Hence, the decrease in bismuth nanoparticle size could effectively increase the ECSA of the electrode. However, besides the size and ECSA effects, the electrode structure and porosity may influence nBi catalysts' activity and selectivity toward CO_2ER [25]. The ECSA and current density are not in a directly proportional relationship, especially at more negative potentials [26]. For example, the ECSA ratio of the nBO-nBi electrode to the mBO-nBi electrode was ~2, but the corresponding CO_2 reduction current ratio was ~1.7 at −0.74 V and 1.1 at −1.08 V. This suggests a comprehensive influence of ECSA and electrode structure on catalyst performance. The nBi electrodes used in this study were porous, presenting a potential mass transfer issue in the electrode membranes. As a result of the smaller primary particles of nBO-nBi, the pores in nBO-nBi should be smaller and more tortuous. Therefore, while the large ECSA of nBO-nBi may provide more catalytic sites, the electrode may face more mass transfer difficulties, especially at larger polarization conditions. In particular, at high overpotentials, when the mass transfer became the rate-determining step, the performance of nBO-nBi might be inferior to that of the mBO-nBi electrode (Fig. 5(d)). In such a case, the local CO_2 concentration in the inner part of the electrode significantly decreased owing to the mass transfer difficulty of CO_2, unlike in the case of water; consequently, the contribution of CO_2ER to the overall electrochemical reaction at the electrode would decrease, and the HER would become increasingly greater with increasing polarization, resulting in a limited formate partial current and a high $FE_{hydrogen}$ (Fig. 5(c)–(d)) [27]. In contrast, at relatively positive potentials, in which the electron transfer step essentially controls the reaction, the nBO-nBi electrode would display a higher formate partial current than the mBO-nBi electrode. Therefore, at relatively negative potentials (high overpotentials), the mBO-nBi electrode outperformed (Fig. 5) the nBO-nBi electrode, as the latter displayed a lower limiting diffusion current for CO_2 reduction to formate (Fig. 5(d)).

As previous works have reported the high catalytic activity of bismuth oxide for the reduction of CO_2 to formate [28–29], the electrocatalytic CO_2ER performance of the pristine nano bismuth oxide (nBO) electrode was tested for comparison (Fig. S4). The catalytic performance of the nBO was comparable to those reported in the literature [28–29] but lower than that of nBO-nBi: (i) at low overpotentials (−0.68

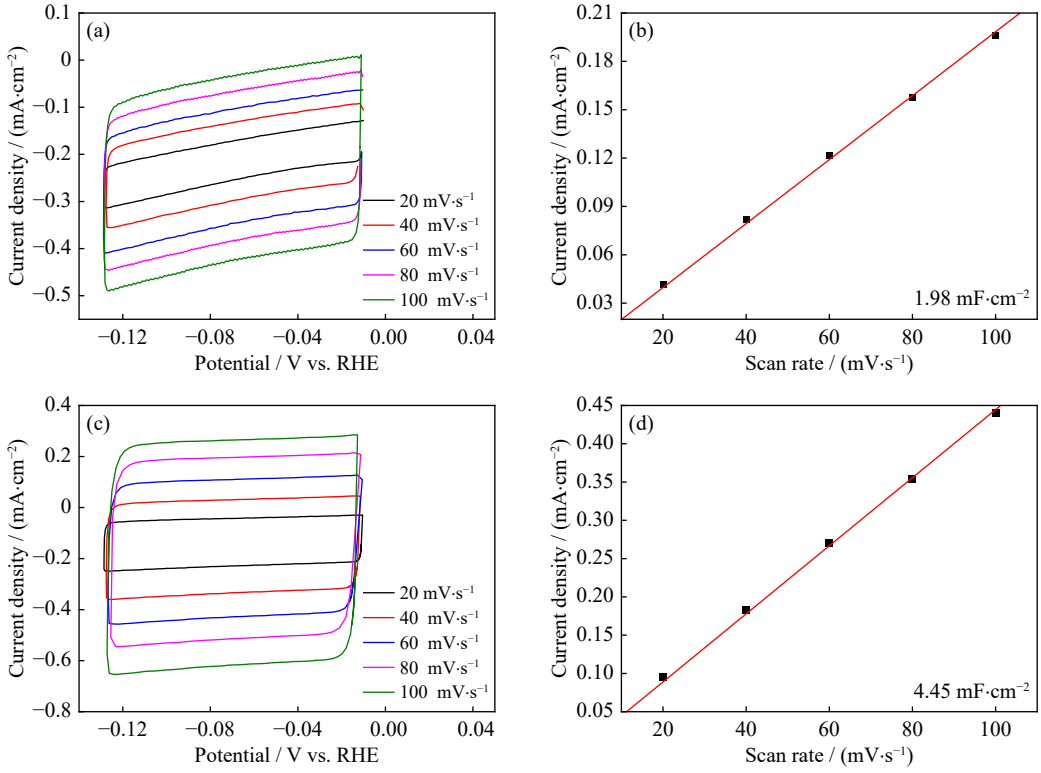

Fig. 6. Cyclic voltammograms (CVs) of the (a) mBO-nBi and (c) nBO-nBi electrodes obtained in a 0.5 M $KHCO_3$ electrolyte. Plots of current densities against the scan rates: (b) mBO-nBi and (d) nBO-nBi. For each CV, the current density was half the gap between anodic and cathodic branches at −0.07 V.

V) when the Bi_2O_3 has not been fully reduced (Fig. S5(a)), the nBO electrode delivered an $FE_{formate}$ of merely 38.5%, only approximately half of the nBO-nBi electrode; (ii) at high overpotentials, the Bi_2O_3 was reduced to Bi (Fig. S5(a)), and the $FE_{formate}$ significantly increased (89% at −0.78 V and 85% at −0.88 V), but it still slightly inferior to that of nBO-nBi (90.4% at −0.78 V and 91.2% at −0.88 V). The SEM images show that the nBO electrodes exhibited markedly different morphologies after CO_2ER at different potentials (Fig. S5(b)–(h)). Therefore, the solid electroreduction of bismuth oxide to nBi in advance would be beneficial for maintaining the consistency of the electrode for a high electrocatalytic CO_2ER performance.

3.3. Investigation of the CO_2 reduction mechanism

Tafel slopes were recorded to elucidate the reduction mechanism of the CO_2ER at nBi electrodes. Typically, the formate formation mechanism includes the following steps [22,30]:

$$CO_2 + * \rightarrow CO_2^* \quad (3)$$

$$CO_2^* + e^- \rightarrow CO_2^{*-} \quad (4)$$

$$CO_2^{*-} + H^+ + e^- \rightarrow HOCO^{*-} \quad (5)$$

$$HOCO^{*-} \rightarrow HOCO^- + * \quad (6)$$

Reaction (3) reflects the adsorption of CO_2 on the catalyst. The nBO-nBi electrode displayed a Tafel slope of 93.1 mV·dec^{-1} (Fig. 7(a)). In contrast, the Tafel slope of the mBO-nBi electrode was relatively large (100.6 mV·dec^{-1}), indicating that increasing the overpotential allows the nBO-nBi electrode to more easily reach a high CO_2 reduction current. The comparison suggests that nBO-nBi exhibited better intrinsic catalytic activity than mBO-nBi. As reported in previous studies, a Tafel slope of 118 mV·dec^{-1} suggests that the CO_2 reduction could be governed by the first electron transfer (reaction (4)) [31]. However, the Tafel slopes of both nBi electrodes were <118 mV·dec^{-1}, suggesting that CO_2 reduction to formate was subject to hybrid control by the first electron transfer and the following hydrogenation step [32]. Bicarbonate ion (HCO_3^-) has been considered the main source of protons according to its pKa (i.e., $-\lg K_a$, and K_a is the acid equilibrium constant of a solution) value (10.33) compared with that of water (15.7) [33]; therefore, the influence of the concentration of HCO_3^- on $j_{formate}$ was investigated. Fig. 7(b) suggests a linear relationship between $j_{formate}$ and HCO_3^- concentration, with a slope of ~1.2, indicating a first-order dependence of HCO_3^- in the rate equation for formate generation. This further suggests that the protonation or the proton-coupled electron transfer reaction (reaction (5)) was involved in the kinetic control of CO_2 reduction to formate [12,34].

Charge-transfer information was explored via electrochemical impedance spectroscopy (Fig. 7(c)), and kinetic parameters were extracted by fitting the impedance spectra with a widely used equivalent circuit (Fig. 7(d)). The charge-transfer resistance (R_{ct}) values of two electrodes were higher

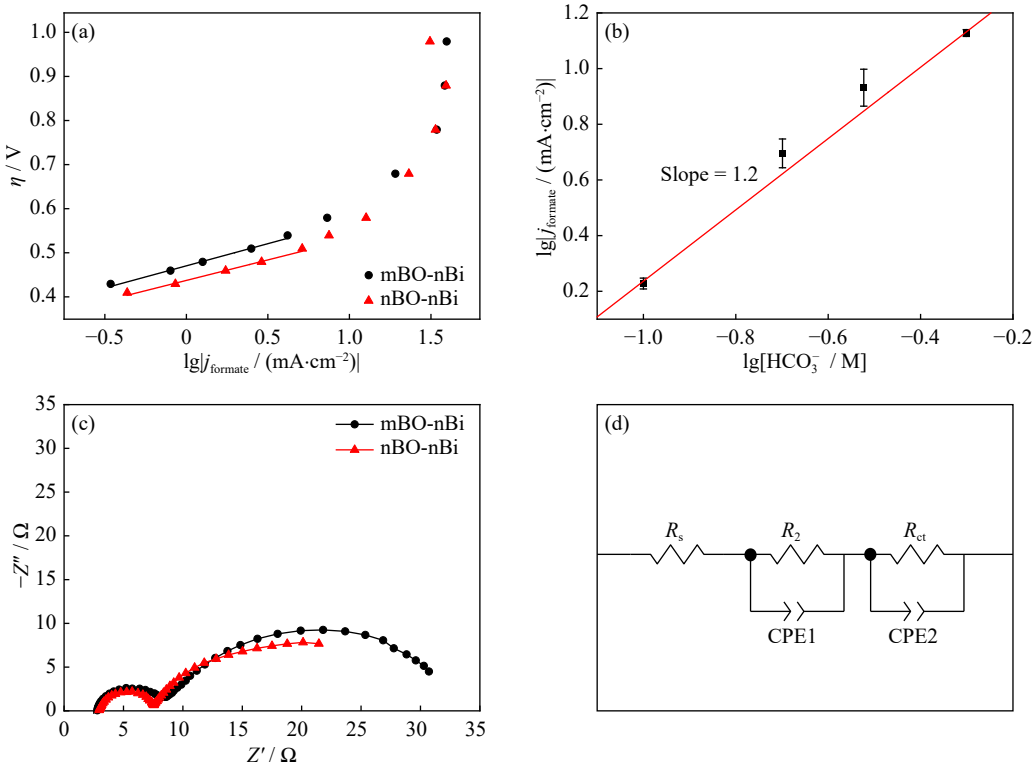

Fig. 7. (a) Tafel plots of formate partial current against overpotential at different nBi catalysts; (b) logarithmic plot of the formate partial current and the $[HCO_3^-]$ concentration at the nBO-nBi electrode (measured at −0.78 V); (c) Nyquist plots of impedance measured at −0.78 V at different nBi catalysts in a CO_2-saturated 0.5 M $KHCO_3$ electrolyte (100 kHz to 1 Hz, amplitude: 10 mV); (d) equivalent circuit used for fitting the data shown in Fig. 7(c).

than the solution and ohmic resistance, indicating that the charge-transfer step at −0.78 V was dominant in the CO_2ER process (Table 1). The mBO-nBi electrode exhibited a higher R_{ct} than the nBO-nBi electrode, consistent with the smaller ECSA of mBO-nBi. However, as discussed above, the formate FE of mBO-nBi during CO_2ER was also lower than that of nBO-nBi, indicating that reducing the particle size of nBi would increase the formate selectivity of the catalyst. These findings align with the Tafel plots. Hence, constructing a three-dimensional connected catalyst layer with small size nBi could improve both reaction kinetics and product selectivity [35].

Table 1. Data obtained after fitting Nyquist plots in Fig. 7(c) (R_s, R_2, and R_{ct} denote solution resistance, ohmic resistance, and charge-transfer resistance, respectively.)

Electrode	R_s / Ω	R_2 / Ω	R_{ct} / Ω
mBO-nBi	2.9	5.4	25.7
nBO-nBi	3.0	4.3	22.8

3.4. Long-term stability of nBi catalysts

Stability is another important criterion in developing electrode catalysts for practical applications. To evaluate the long-term stability of the prepared nBi catalysts, continuous electrolytic reduction of CO_2 was performed through the application of a potential of −0.78 V for 20 h. Some slight fluctuations of current density occurred during the electrolysis process because H_2 and CO were often generated during the CO_2ER process (Fig. 8(a) and (b)). The adsorption and evolution of gas generally lead to current fluctuation, and the higher the gas generation current, the larger the current fluctuation [7,28]. During the long-time CO_2 reduction, the total current of both electrodes revealed no pronounced attenuation, but the $FE_{formate}$ of the mBO-nBi electrode decreased (Fig. 8(a)), with a retention of 78%. However, the nBO-nBi electrode performed stably (Fig. 8(b)), with almost no $FE_{formate}$ change observed during the 20 h electrolysis.

After long-term electrolysis, the electrodes were analyzed via XRD and SEM. Before and after the electrolysis, none of

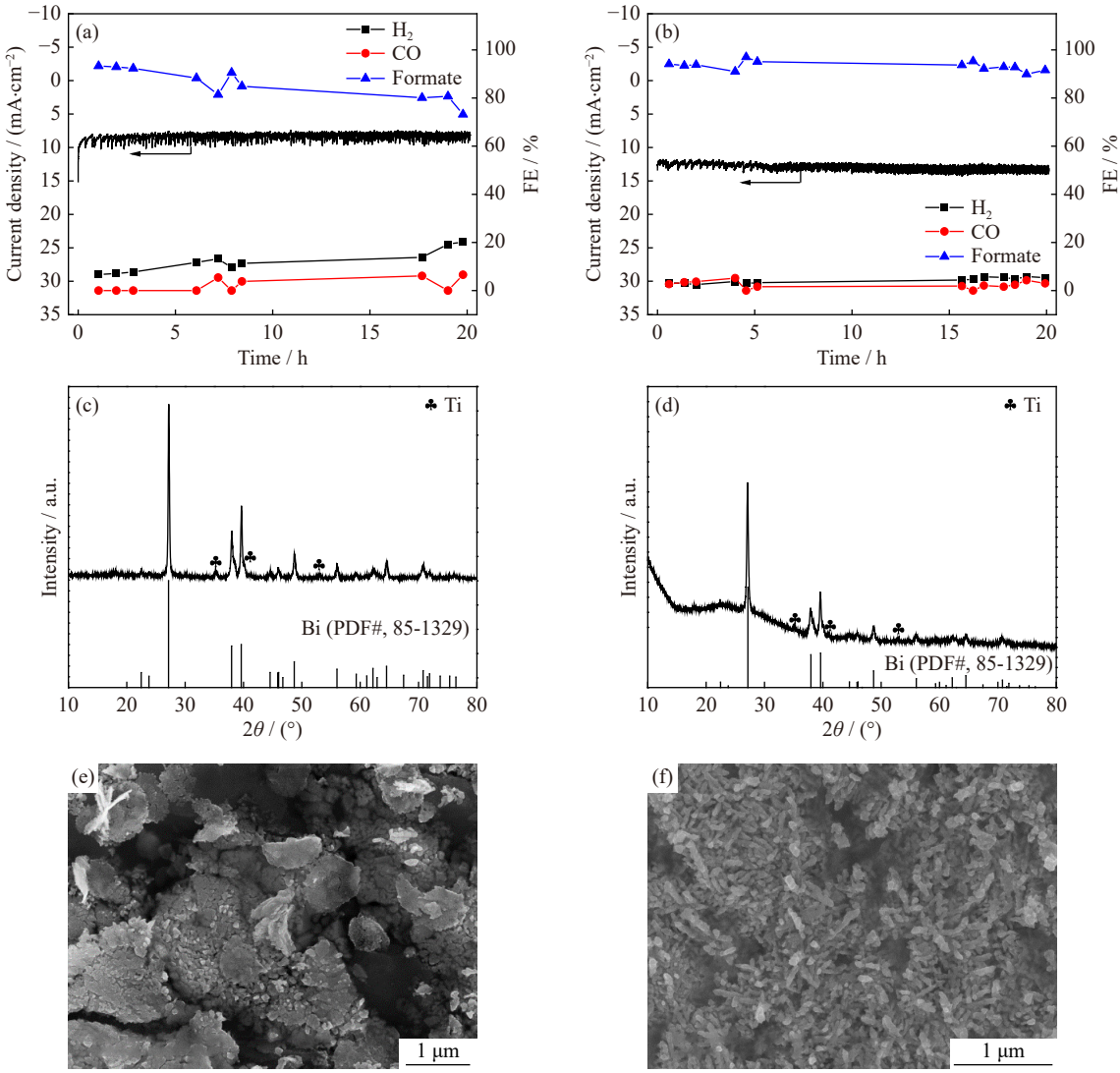

Fig. 8. Total current and product efficiencies during electrolysis of CO_2 at −0.78 V at the (a) mBO-nBi and (b) nBO-nBi electrodes. XRD patterns of (c) mBO-nBi and (d) nBO-nBi after the 20 h electrolysis of CO_2 at −0.78 V; (e, f) SEM images of the electrodes characterized in (c) and (d), respectively.

the electrodes exhibited any change in XRD diffraction peaks, indicating they were phase-stable during the electrolysis (Fig. 8(c) and (d)). The SEM results indicate that the particle sizes of mBO-nBi (Fig. 8(e) vs. Fig. 3(a)) and nBO-nBi (Fig. 8(f) vs. Fig. 3(c)) increased after the 20 h electrolysis. The size increase was probably the main reason for the decrease in the formate selectivity of the mBO-nBi electrode. In contrast, while the Bi nanoparticles in the nBO-nBi electrode agglomerated and the size of the Bi particle increased, the $FE_{formate}$ changed little, suggesting that there was a size range for the Bi to achieve a high $FE_{formate}$; for example, both the mBO-nBi (~80 nm) and nBO-nBi (30–50 nm) electrodes exhibited similar $FE_{formate}$ values in the potential range of −0.65 to −1.0 V. However, the stability test results suggest that a further increase in the particle size of nBi beyond the aforementioned range would result in a rapid drop in $FE_{formate}$. Studies have often attributed the morphological changes of electrode catalysts after long-term electrolysis to the surface reorganization of the catalysts, probably induced by the surface adsorption/desorption, related to the strong interaction between the Bi metal and CO_2 or its derivations [12,26,36]. The long-term instability of the nBi catalysts needs to be investigated further. Nevertheless, during the 20 h CO_2ER test, the nBO-nBi electrode displayed high activity, durability, and selectivity. Moreover, the mBO-nBi and nBO-nBi electrodes exhibited comparable and even higher catalytic activity compared with other formate catalysts recently reported in the literature (Table S1) [37–40]. This demonstrates the application potential of the oxide-derived nBi catalysts for CO_2ER.

4. Conclusion

In summary, a nanostructured Bi catalyst was prepared through the direct solid electroreduction of Bi_2O_3 in a K_2CO_3 solution. Both mBO-nBi and nBO-nBi electrodes, derived from micronized and nanosized bismuth oxide, respectively, exhibited a hierarchical structure and an integrated conductive network and demonstrated high CO_2 reduction activity and formate selectivity. They achieved high formate FEs (>80%) in a wide potential window, between −0.63 and −0.98 V for the nBO-nBi electrode and between −0.65 and −1.08 V for the mBO-nBi electrode. However, at lower polarization conditions, nBO-nBi exhibited a higher formate production rate and FE than mBO-nBi. This suggests the intrinsic high catalytic activity of the smaller nanoscale Bi particles toward CO_2 reduction to formate. This study provides a novel approach for fabricating interlinked nanostructured catalysts, which may prove helpful for designing high-efficiency catalysts in the future.

Acknowledgements

This work was financially supported by the National Natural Science Foundation of China (Nos. 22072110 and 21872107) and the Key Research and Development Projects of Hubei Province, China (2022BAA083).

Conflict of Interest

The authors declare that they have no known competing financial interests or personal relationships that could have appeared to influence the work reported in this paper.

Supplementary Information

The online version contains supplementary material available at https://doi.org/10.1007/s12613-023-2770-y

References

[1] Z.Y. Sun, T. Ma, H.C. Tao, Q. Fan, and B.X. Han, Fundamentals and challenges of electrochemical CO_2 reduction using two-dimensional materials, *Chem*, 3(2017), No. 4, p. 560.

[2] N. Han, P. Ding, L. He, Y.Y. Li, and Y.G. Li, Promises of main group metal-based nanostructured materials for electrochemical CO_2 reduction to formate, *Adv. Energy Mater.*, 10(2020), No. 11, art. No. 1902338.

[3] R. Kortlever, J. Shen, K.J.P. Schouten, F. Calle-Vallejo, and M.T.M. Koper, Catalysts and reaction pathways for the electrochemical reduction of carbon dioxide, *J. Phys. Chem. Lett.*, 6(2015), No. 20, p. 4073.

[4] X. Chen, Y. Liu, and J.W. Wu, Sustainable production of formic acid from biomass and carbon dioxide, *Mol. Catal.*, 483(2020), art. No. 110716.

[5] Z.N. Yang, F.E. Oropeza, and K.H.L. Zhang, P-block metal-based (Sn, In, Bi, Pb) electrocatalysts for selective reduction of CO_2 to formate, *APL Mater.*, 8(2020), No. 6, art. No. 060901.

[6] S.Y. Yang, M.H. Jiang, W.J. Zhang, *et al.*, *In situ* structure refactoring of bismuth nanoflowers for highly selective electrochemical reduction of CO_2 to formate, *Adv. Funct. Mater.*, 33(2023), No. 37, art. No. 2301984.

[7] W.J. Zhang, S.Y. Yang, M.H. Jiang, *et al.*, Nanocapillarity and nanoconfinement effects of pipet-like bismuth@carbon nanotubes for highly efficient electrocatalytic CO_2 reduction, *Nano Lett.*, 21(2021), No. 6, p. 2650.

[8] R. Zhou, N. Han, and Y.G. Li, Recent advances in bismuth-based CO_2 reduction electrocatalysts, *J. Electrochem.*, 25(2019), No. 4, p. 445.

[9] H. Yang, N. Han, J. Deng, *et al.*, Selective CO_2 reduction on 2D mesoporous Bi nanosheets, *Adv. Energy Mater.*, 8(2018), No. 35, art. No. 1801536.

[10] P.L. Lu, D.L. Gao, H.Y. He, *et al.*, Facile synthesis of a bismuth nanostructure with enhanced selectivity for electrochemical conversion of CO_2 to formate, *Nanoscale*, 11(2019), No. 16, p. 7805.

[11] Y.N. Zhang, D.F. Niu, S.Z. Hu, and X.S. Zhang, Recent progress on enhancing effect of nanosized metals for electrochemical CO_2 reduction, *J. Electrochem.*, 26(2020), No. 4, p. 495.

[12] D. Wu, G. Huo, W.Y. Chen, X.Z. Fu, and J.L. Luo, Boosting formate production at high current density from CO_2 electroreduction on defect-rich hierarchical mesoporous Bi/Bi_2O_3 junction nanosheets, *Appl. Catal. B: Environ.*, 271(2020), art. No. 118957.

[13] P.P. Su, W.B. Xu, Y.L. Qiu, T.T. Zhang, X.F. Li, and H.M. Zhang, Ultrathin bismuth nanosheets as a highly efficient CO_2 reduction electrocatalyst, *ChemSusChem*, 11(2018), No. 5, p. 848.

[14] L. Zhang, Z.Y. Wang, N. Mehio, X.B. Jin, and S. Dai, Thickness- and particle-size-dependent electrochemical reduction of

carbon dioxide on thin-layer porous silver electrodes, *ChemSusChem*, 9(2016), No. 5, p. 428.

[15] G.R. Jia, Y. Wang, M.Z. Sun, *et al*., Size effects of highly dispersed bismuth nanoparticles on electrocatalytic reduction of carbon dioxide to formic acid, *J. Am. Chem. Soc.*, 145(2023), No. 25, p. 14133.

[16] M. Azuma, K. Hashimoto, M. Hiramoto, M. Watanabe, and T. Sakata, Electrochemical reduction of carbon dioxide on various metal electrodes in low-temperature aqueous $KHCO_3$ media, *J. Electrochem. Soc.*, 137(1990), No. 6, p. 1772.

[17] Q. Lu, J. Rosen, Y. Zhou, *et al*., A selective and efficient electrocatalyst for carbon dioxide reduction, *Nat. Commun.*, 5(2014), art. No. 3242.

[18] G.O. Barasa, T.S. Yu, X.L. Lu, *et al*., Electrochemical training of nanoporous Cu-In catalysts for efficient CO_2-to-CO conversion and high durability, *Electrochim. Acta*, 295(2019), p. 584.

[19] L. Li, F.F. Cai, F.X.Y. Qi, and D.K. Ma, Cu nanowire bridged Bi nanosheet arrays for efficient electrochemical CO_2 reduction toward formate, *J. Alloys Compd.*, 841(2020), art. No. 155789.

[20] F.P. García de Arquer, O.S. Bushuyev, P. de Luna, *et al*., 2D metal oxyhalide-derived catalysts for efficient CO_2 electroreduction, *Adv. Mater.*, 30(2018), No. 38, art. No. 1802858.

[21] T. Burdyny, P.J. Graham, Y.J. Pang, *et al*., Nanomorphology-enhanced gas-evolution intensifies CO_2 reduction electrochemistry, *ACS Sustainable Chem. Eng.*, 5(2017), No. 5, p. 4031.

[22] K. Fan, Y.F. Jia, Y.F. Ji, *et al*., Curved surface boosts electrochemical CO_2 reduction to formate via bismuth nanotubes in a wide potential window, *ACS Catal.*, 10(2020), No. 1, p. 358.

[23] C.W. Li and M.W. Kanan, CO_2 reduction at low overpotential on Cu electrodes resulting from the reduction of thick Cu_2O films, *J. Am. Chem. Soc.*, 134(2012), No. 17, p. 7231.

[24] W.J. Yan, J.T. Zhang, A.J. Lü, S.L. Lu, Y.W. Zhong, and M.Y. Wang, Self-supporting and hierarchically porous Ni_xFe–S/$NiFe_2O_4$ heterostructure as a bifunctional electrocatalyst for fluctuating overall water splitting, *Int. J. Miner. Metall. Mater.*, 29(2022), No. 5, p. 1120.

[25] W.Q. Lai, Y.T. Liu, M.M. Zeng, *et al*., One-step electrochemical dealloying of 3D Bi-continuous micro-nanoporous bismuth electrodes and CO_2RR performance, *Nanomaterials*, 13(2023), No. 11, art. No. 1767.

[26] S. Kim, W.J. Dong, S. Gim, *et al*., Shape-controlled bismuth nanoflakes as highly selective catalysts for electrochemical carbon dioxide reduction to formate, *Nano Energy*, 39(2017), p. 44.

[27] M.R. Singh, E.L. Clark, and A.T. Bell, Effects of electrolyte, catalyst, and membrane composition and operating conditions on the performance of solar-driven electrochemical reduction of carbon dioxide, *Phys. Chem. Chem. Phys.*, 17(2015), No. 29, p. 18924.

[28] S. Liu, X.F. Lu, J. Xiao, X. Wang, and X.W.D. Lou, Bi_2O_3 nanosheets grown on multi-channel carbon matrix to catalyze efficient CO_2 electroreduction to HCOOH, *Angew. Chem. Int. Ed.*, 58(2019), No. 39, p. 13828.

[29] Q.F. Gong, P. Ding, M.Q. Xu, *et al*., Structural defects on converted bismuth oxide nanotubes enable highly active electrocatalysis of carbon dioxide reduction, *Nat. Commun.*, 10(2019), No. 1, art. No. 2807.

[30] X. Zhang, J. Fu, Y.Y. Liu, X.D. Zhou, and J.L. Qiao, Bismuth anchored on MWCNTs with controlled ultrafine nanosize enables high-efficient electrochemical reduction of carbon dioxide to formate fuel, *ACS Sustainable Chem. Eng.*, 8(2020), No. 12, p. 4871.

[31] Y.L. Xing, H.H. Chen, Y. Liu, *et al*., A phosphate-derived bismuth catalyst with abundant grain boundaries for efficient reduction of CO_2 to HCOOH, *Chem. Commun.*, 57(2021), No. 12, p. 1502.

[32] P.L. Deng, H.M. Wang, R.J. Qi, *et al*., Bismuth oxides with enhanced bismuth–oxygen structure for efficient electrochemical reduction of carbon dioxide to formate, *ACS Catal.*, 10(2020), No. 1, p. 743.

[33] S. Zhang, P. Kang, and T.J. Meyer, Nanostructured tin catalysts for selective electrochemical reduction of carbon dioxide to formate, *J. Am. Chem. Soc.*, 136(2014), No. 5, p. 1734.

[34] X.Y. Wang, Z.Y. Wang, and X.B. Jin, Nanoporous bismuth for the electrocatalytic reduction of CO_2 to formate, *Phys. Chem. Chem. Phys.*, 23(2021), No. 35, p. 19195.

[35] W.J. Dong, C.J. Yoo, and J.L. Lee, Monolithic nanoporous In–Sn alloy for electrochemical reduction of carbon dioxide, *ACS Appl. Mater. Interfaces*, 9(2017), No. 50, p. 43575.

[36] F.H. Zhang, C.Z. Chen, S.L. Yan, J.H. Zhong, B. Zhang, and Z.M. Cheng, Cu@Bi nanocone induced efficient reduction of CO_2 to formate with high current density, *Appl. Catal. A*, 598(2020), art. No. 117545.

[37] X.W. An, S.S. Li, A. Yoshida, *et al*., Bi-doped SnO nanosheets supported on Cu foam for electrochemical reduction of CO_2 to HCOOH, *ACS Appl. Mater. Interfaces*, 11(2019), No. 45, p. 42114.

[38] Q. Yang, Q.L. Wu, Y. Liu, *et al*., Novel Bi-doped amorphous SnO_x nanoshells for efficient electrochemical CO_2 reduction into formate at low overpotentials, *Adv. Mater.*, 32(2020), No. 36, art. No. 2002822.

[39] M.Y. Fan, S. Prabhudev, S. Garbarino, *et al*., Uncovering the nature of electroactive sites in nano architectured dendritic Bi for highly efficient CO_2 electroreduction to formate, *Appl. Catal. B*, 274(2020), art. No. 119031.

[40] Y.T. Wang, L. Cheng, J.Z. Liu, *et al*., Rich bismuth–oxygen bonds in bismuth derivatives from Bi_2S_3 pre-catalysts promote the electrochemical reduction of CO_2, *ChemElectroChem*, 7(2020), No. 13, p. 2864.